THE EUROPEAN
PHYSICAL JOURNAL B

Random walks in correlated diffusivity landscapes

Adrian Pacheco-Pozo[1,a] and Igor M. Sokolov[1,2,b]

[1] Institut für Physik, Humboldt-Universität zu Berlin, Newtonstraße 15, 12489 Berlin, Germany
[2] IRIS Adlershof, Zum Großen Windkanal 2, 12489 Berlin, Germany

Abstract. In recent years, several experiments have highlighted a new type of diffusion anomaly, which was called Brownian yet non-Gaussian diffusion. In systems displaying this behavior, the mean squared displacement of the diffusing particles grows linearly in time, like in a normal diffusion, but the distribution of displacements is non-Gaussian. In situations when the convergence to Gaussian still takes place at longer times, the probability density of the displacements may show a persisting peak around the distribution's mode, and the pathway of convergence to the Gaussian is unusual. One of the theoretical models showing such a behavior corresponds to a disordered system with local diffusion coefficients slowly varying in space. While the standard pathway to Gaussian, as proposed by the Central Limit Theorem, would assume that the peak, under the corresponding rescaling, smoothens and lowers in course of the time, in the model discussed, the peak, under rescaling, narrows and stays sharp. In the present work, we discuss the nature of this peak. On a coarse-grained level, the motion of the particles in the diffusivity landscape is described by continuous time random walks with correlations between waiting times and positions. The peak is due to strong spatiotemporal correlations along the trajectories of diffusing particles. Destroying these correlations while keeping the temporal structure of the process intact leads to the decay of the peak. We also note that the correlated CTRW model reproducing serial correlations between the waiting times along the trajectory fails to quantitatively reproduce the shape of the peak even for the decorrelated motion, while being quite accurate in the wings of the PDF. This shows the importance of high-order temporal correlations for the peak's formation.

1 Introduction

The erratic motion of particles diffusing in a fluid medium (Brownian motion) has drawn considerable attention of scientists since Robert Brown first systematically investigated it [1]. Einstein [2] was the first to propose a mathematical description of this type of motion (see [3] for a detailed historical account). Einstein, who essentially did not know about Brownian motion, found out that such a phenomenon is an inavoidable consequence of the kinetic theory of heat and closely connected it to diffusion. In this picture of what we now call *normal diffusion*, the particles' motion possesses two important properties [4]: (i) the mean square displacement (MSD) of the particles from their initial position grows linearly in time,

$$\langle \mathbf{r}(t)^2 \rangle = 2dDt \qquad (1)$$

(with d being the dimension of space, and D being the diffusion coefficient), and (ii) the probability den-

sity function (PDF) of the particles' displacements at a given time follows a Gaussian distribution

$$p(\mathbf{r}, t) = \frac{1}{(4\pi Dt)^{d/2}} \exp\left(-\frac{\mathbf{r}^2}{4Dt}\right). \qquad (2)$$

The properties (1) and (2) were tested in many experiments, and their confirmation laid a solid foundation to our understanding of the atomistic structure of matter [5]. The random walk approach used by Einstein assumed that one can approximate the particle's motion by a sequence of independent steps in random directions under the condition that the times necessary to make a step are the same, and the displacement in a single step has a finite second moment. This approach was closely mirrored in many early experiments using stroboscopic measurements. Independently of Einstein, Smoluchowski [6] presented a more formal mathematical description of the Brownian motion which led to the same results as Einstein's, and set the ground to a new branch of probability theory concerning the diffusion processes [7]. After Einstein and Smoluchowski, Langevin [8] proposed a new mathematical tool for the description of the particle's motion, the stochastic differential equation.

[a] e-mail: adrian.pacheco@physik.hu-berlin.de (corresponding author)

[b] e-mail: igor.sokolov@physik.hu-berlin.de

The standard picture corresponds to the tracer's motion in a homogeneous, quiescent fluid. In the course of time, many deviations from this kind of behavior were found for other media. Numerous experiments on transport in complex media (disordered solids, rocks, biological media, etc.) showed that, instead of a linear time dependence as given by Eq. (1), the MSD often follows a power-law time-dependence $\langle \mathbf{r}(t)^2 \rangle \propto t^\gamma$, with $0 < \gamma < 1$ (subdiffusion) or $1 < \gamma < 2$ (superdiffusion). A system whose MSD shows such a time dependence is said to exhibit *anomalous diffusion*. Depending on the specific case, different mathematical models have been proposed to describe this anomalous behavior by focusing on different aspects of the motion [9–14]. Some classical models are: the uncorrelated continuous time random walks (CTRW) with power-law waiting time distributions, the fractional Brownian motion, and Lévy walks and Lévy flights. The PDF in these models may or may not be Gaussian. An alternative model to uncorrelated CTRW which also produce anomalous behavior is the annealed transit time model (ATTM) [15], which introduces the idea of random diffusivities. Several considered cases include variants or combinations of different sources of anomalies: thus, diffusion in strongly fluctuating Gaussian random potentials is considered in [16], and a combination of a random potential and viscoelastic memory as described by the generalized Langevin dynamics was discussed in [17,18].

Several recent experiments [19–35] reported a new type of diffusion in which the MSD grows linearly in time, like in the normal diffusion, yet the PDF of displacements shows considerable deviations from the Gaussian shape. Usually, the PDF of displacements is well described by a Laplace (two-sided exponential) distribution. This behavior was called Brownian, yet non-Gaussian (BnG) diffusion [22]. Some of the corresponding systems show a crossover from the non-Gaussian distribution to a Gaussian one at long times [19,34]. In several cases [19,22,23,28,30–35], for times at which the crossover takes place, the PDF presents a peak close to its mode. This peak resembles a part of the initial Laplace distribution, while the parts of the distribution further from its mode have already a more or less Gaussian shape. This peak can be also seen in several theoretical works [36,37], whereas in other closely related works, it is absent [38–40].

Many of the systems in which the BnG diffusion is observed are pertinent to soft matter, and almost all of the experimental systems with BnG diffusion may show a great deal of spatial and temporal inhomogeneity, or disorder. Thus, the medium in which the particle moves may be spatially heterogeneous, or change in time. The properties of the diffusing tracer may change in time as well.

Different assumptions about the heterogeneity involved lead to different classes of models which were proposed for the description of BnG diffusion. The most popular class corresponds to the diffusing diffusivity (DD) models, see e.g., [41–45]. They assume slow random changes of the diffusion coefficient in time. The particular variant of the model used in [43] will be called "the minimal model" of diffusing diffusivity in what follows. Due to the versatility of this particular variant, it has also been applied to the study of fractional Brownian motion, a model presenting long-ranged time dependences [46]. Another model describing BnG diffusion is the diffusivity landscape model (DLM) [47], which considers that the diffusion coefficient varies slowly in space.

The possible connection between the diffusing diffusivity and DLM was stated in Ref. [43]: the temporal randomness of the diffusion coefficient can be considered as stemming from its spatial change along the trajectory of a diffusing particle, so that the "minimal model" is a kind of a mean-field approximation for the case of spatial changes. Even if the DD and DL models are gauged in such a way that they reproduce the main features of the phenomenon, their predictions differ in some details. Looking particularly into these details may deliver valuable experimental insights into the kind of disorder involved. Thus, the DLM (and other models with correlated spatial disorder like the one discussed in [48,49], not necessarily exhibiting the BnG behavior) show a pronounced central peak at the mode of the PDF of particles' displacements. This central peak is, however, absent in the minimal model. The existence of this central peak in [48] was immediately connected to the correlated nature of disorder.

Recently, in Ref. [50], we concentrated on the behavior of the PDF of displacements close to its mode and showed that the PDF of displacements in several classical strongly disordered systems displays such a peak at its center. The behavior of this central peak is quite peculiar, since its presence shows that the convergence to a Gaussian (i.e., normal) behavior under homogenization may follow a different pathway than the one commonly known from the Central Limit Theorem (CLT) applied to sums of many independent, identically distributed (i.i.d.) random variables following some continuous distribution (in our case, this should be the short-time Laplace one). This standard situation suggests that the initially sharp peak would smoothen and be lowered. However, under homogenization, the central peak in the considered classical strongly disordered systems gets narrower under the rescaling $\mathbf{r} \to \mathbf{r}/\sqrt{t}$, $p \to t^{d/2}p$ implied by the CLT, while approximately keeping the height. Passing from the spatially disordered systems to their mean-filed counterparts (like the corresponding CTRWs, or the minimal model) restores the standard convergence pathway like the one predicted by the CLT.

The differences in the convergence pathways have to do with the fact that some important local information about the system is erased when passing to the pre-averaged (mean-field) description. Now, one could ask, what is the important information erased? In the present work, we try to answer this question by simulating the particles' trajectories in DLM (described as a continuous-time random walk of particles on a lattice with position-dependent waiting times) and erase the correlations between the waiting times and posi-

tions, while fully preserving the temporal structure of the walk. The result of the discussion shows that the existence of the persistent peak is connected to spatiotemporal correlations, and destroying them (while fully preserving the temporal structure of the problem) leads to a different kind of behavior. We note that the answer to this question may apply in other similar situations in strongly disordered systems.

The article is structured as follows. In Sect. 2, we revisit the diffusivity landscape model being the base of our investigation. Section 3 explores the idea that the DLM presents strong spariotemporal correlations which ultimately leads to the PDF exhibiting a central peak. We show that destroying these spatiotemporal correlations while fully preserving the temporal structure of steps reproduces the PDF in DLM at short times, but leads to lowering and disappearing of the peak at long ones. Section 4 provides a CTRW model with correlated waiting times, which partially reproduces the behavior found in this decorrelated DLM model, but fails to fully describe the situation. In Sect. 5, we discuss the role of the particular shape of the correlation function of diffusivities assumed in DLM by considering a slightly different model. Finally, Sect. 6 presents the concluding remarks.

2 Diffusivity landscape model

In what follows, we use the model proposed by Postnikov et al. [47] which assumes the particles' diffusion in a heterogeneous medium modeled by a correlated diffusivity landscape $D(\mathbf{r})$. This motion is described by the force-free Langevin equation with multiplicative noise

$$\frac{d}{dt}\mathbf{r} = \sqrt{2D(\mathbf{r})}\,\boldsymbol{\xi}(t), \qquad (3)$$

with $\boldsymbol{\xi}(t)$ being a Gaussian white noise with $\langle\boldsymbol{\xi}(t)\rangle = 0$ and $\langle\xi_\mu(t)\xi_\nu(t')\rangle = \delta_{\mu\nu}\delta(t - t')$ with μ, ν representing Cartesian coordinates. This Langevin equation corresponds to the Fokker–Planck equation

$$\frac{\partial}{\partial t}p(\mathbf{r},t) = \nabla[(1-\alpha)\nabla D(\mathbf{r}) + D(\mathbf{r})\nabla]p(\mathbf{r},t), \quad (4)$$

with α being the interpretation parameter taking values in the interval $0 \leq \alpha \leq 1$. The interpretation parameter arises because of the different ways in which one can integrate Eq. (3) (see e.g., [51] for a comprehensive discussion). Among all the different values the interpretation parameter could take, three values stand from the rest [52]: $\alpha = 0, 1/2$ and 1, which are known as the interpretation of Ito, Stratonovich and Hänggi-Klimontovich, respectively. Note that assuming different interpretations (all complying with the idea of pure diffusivity landscape, without any external potential) leads to different stationary probability densities $p(\mathbf{r},t)$, which influence the sampling of trajectories of diffusing particles. The authors of [47] asked, under which condition would Eq. (4) describe the BnG diffusion, and found out that the two following conditions should be met. First, Eq. (3) without external potential must be interpreted in the Ito sense ($\alpha = 0$; then, of course, any other interpretation can be used by introducing the corresponding deterministic force [51]), and second, initial positions of diffusing particles must be sampled from the equilibrium distribution. Taking as a "stylized fact" that the PDF at short times has been observed to follow a Laplace distribution [19–35], one can then show that the single-point PDF of the diffusion coefficients in the corresponding landscape should be given by a Gamma distribution:

$$p(D) = \frac{\beta^\beta}{\Gamma(\beta)}\frac{1}{\overline{D}}\left(\frac{D}{\overline{D}}\right)^{\beta-1}\exp\left(-\beta\frac{D}{\overline{D}}\right), \qquad (5)$$

where $\Gamma(\cdot)$ is a Gamma function, and β and $\overline{D}$ are shape parameters dependent on the dimension of space.

In what follows, we will concentrate on the two-dimensional situation, for which $\beta = 5/2$ and $\overline{D} = 5D_0/3$, with D_0 being the sampled diffusion coefficient, i.e., the one defining the slope of the "experimental" MSD assumed to strictly follow the linear dependence $\langle\mathbf{r}(t)^2\rangle = 2dD_0t$ [47].

A finite-difference discretization of the Fokker–Planck equation, Eq. (4), with $\alpha = 0$ on a square lattice with lattice constant a leads to a master equation (see Eq. (6) below) which, in its turn, defines a random walk scheme. The corresponding random walks are exactly what will be simulated in what follows.

For $\alpha = 0$, Eq. (4) can be rewritten in the form

$$\frac{\partial}{\partial t}p(\mathbf{r},t) = \Delta[D(\mathbf{r})p(\mathbf{r},t)],$$

and its discrete version is

$$\frac{d}{dt}p_i(t) = \sum_{k=1}^{4}\frac{D_{j_k}}{a^2}p_{j_k}(t) - \frac{4D_i}{a^2}p_i(t). \qquad (6)$$

Here, the discretization point i corresponds to coordinates (x_i, y_i) on a rectangular grid with the lattice constant a, and points j_k are the four nearest neighbors of the lattice point i.

Under the above discretization, the random diffusivity field at each lattice point translates into correlated values of local parameters $D_i \equiv D(x_i, y_i)$, which are generated according to the following algorithm, Ref. [47]: one begins by constructing an array of independent Gaussian random variables G_i with zero mean and unit variance. Then one generates a correlated Gaussian field $\widehat{G}_i$ by applying the Fourier filtering method [53] to G_i. Like in [47], we take the correlation function of the correlated field to follow

$$\rho(\mathbf{r}_{ij}) = \langle\widehat{G}_i\widehat{G}_j\rangle = \exp\left(-\frac{\mathbf{r}_{ij}^2}{2\lambda^2}\right), \qquad (7)$$

with λ being the correlation length, and $\mathbf{r}_{ij}$ the Euclidean distance between lattice points i and j. We note that the choice of Eq. (7) is not dictated by any physical reasons, but by the ease of numerical implementation and further calculations. In Sect. 5, we will explore the consequences of changing the correlation function of the diffusivity landscape by considering a checkerboard-like diffusivity landscape.

Finally, the correlated Gaussian field $\widehat{G}_i$ is transformed into the Γ-distributed diffusivity landscape D_i by performing a probability transformation:

$$D_i = f(\widehat{G}) = F_\beta^{-1}\left\{\frac{1}{2}\left[1 - \mathrm{erf}\left(\frac{\widehat{G}}{\sqrt{2}}\right)\right]\right\}, \quad (8)$$

where $\mathrm{erf}(\cdot)$ is the error function and $F_\beta^{-1}(x)$ is the inverse of the cumulative distribution function (CDF) $F_\beta(D)$ for the PDF given by Eq. (5), which is given by

$$F_\beta(D) = \int_0^D p(D')dD' = \frac{1}{\Gamma(\beta)}\gamma\left(\beta, \beta\frac{D}{\overline{D}}\right),$$

with $\gamma(\cdot, \cdot)$ being the lower incomplete Gamma function. The procedure above generates a diffusivity landscape D_i whose correlation function follows from that of the correlated Gaussian field, Eq. (7), by a transformation which will be discussed in Sect. 4.1.

Figure 1 shows a realization of the diffusivity landscape D_i for a lattice of 256×256 with $a = 1$, $D_0 = 1$ and $\lambda = 10$.

Let us now return to our Eq. (6). Defining the transition rates as

$$\omega_{i\to j} = \frac{D_i}{a^2} = \frac{1}{4}\left(\frac{a^2}{4D_i}\right)^{-1} = \frac{1}{4}\frac{1}{\tau_i},$$
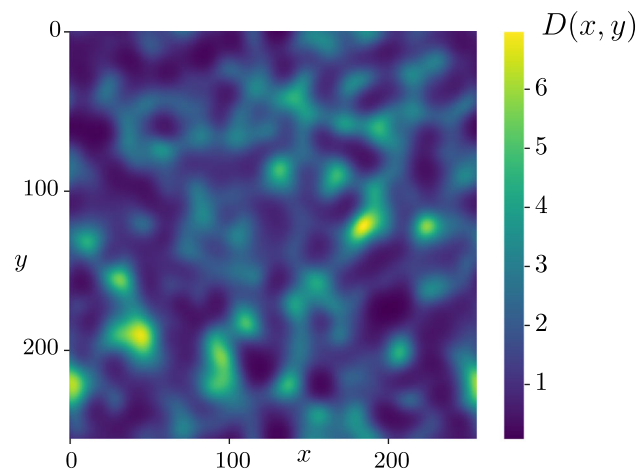
Fig. 1 A two-dimensional realization of the diffusivity landscape $D(\mathbf{r})$ in the diffusivity landscape model. It corresponds to a 256×256 lattice with correlation length $\lambda = 10$ and sampled diffusion coefficient $D_0 = 1$

with

$$\tau_i = \frac{a^2}{4D_i} \quad (9)$$

being the mean waiting time at a site, and 1/4 corresponding to the probability to choose one of the four neighbors to jump to. We put Eq. (6) into a standard form of a master equation

$$\frac{d}{dt}p_i(t) = \sum_{k=1}^{4}\omega_{j_k\to i}p_{j_k}(t) - \sum_{k=1}^{4}\omega_{i\to j_k}p_i(t),$$

which can be rewritten as

$$\frac{d}{dt}p_i(t) = \frac{1}{4}\sum_{k=1}^{4}\frac{1}{\tau_{j_k}}p_{j_k}(t) - \frac{1}{\tau_i}p_i(t). \quad (10)$$

In Ref. [47], Eq. (10) was solved using the forward Euler method. Here, we employ another approach.

Note that Eq. (10) which arose from the discretization of the Fokker–Planck equation corresponds to a lattice model with static random traps [54,55]. Like in Ref. [50], we use the fact that the master equation (10) corresponds to a CTRW with a site-dependent exponential distribution of waiting times on the sites. Thus, to solve the master equation, i.e., to obtain the evolution of the PDF, we generate random walk trajectories whose waiting times follow the exponential waiting time density

$$\psi(t|\tau_i) = \frac{1}{\tau_i}\exp\left(-\frac{t}{\tau_i}\right),$$

with τ_i given by Eq. (9). Taking the lattice spacing to be the length unit of the problem ($a = 1$), we get

$$\psi(t|D_i) = 4D_i\exp\left(-4D_it\right). \quad (11)$$

Note that the single-step displacements in our CTRW are i.i.d. random variables (each step has a unit length and arbitrary, random direction), while waiting times are not independent since D_i at neighboring points are correlated. An illustration of the procedure to generate random trajectories can be seen in panel (a) of Fig. 2. As we shall see, this alternative method allows us to study the role of space–time correlations in the DLM, which would be impossible to do by solving the ordinary differential equations (ODEs). Moreover, generating random trajectories is considerably less computationally expensive than solving ODEs, and allows us to have much better statistics of the desired quantities.

3 Space–time correlations

In the last decades, several correlated CTRW models were proposed which led to interesting behaviors [56–58]. However, all these correlated models focus only on
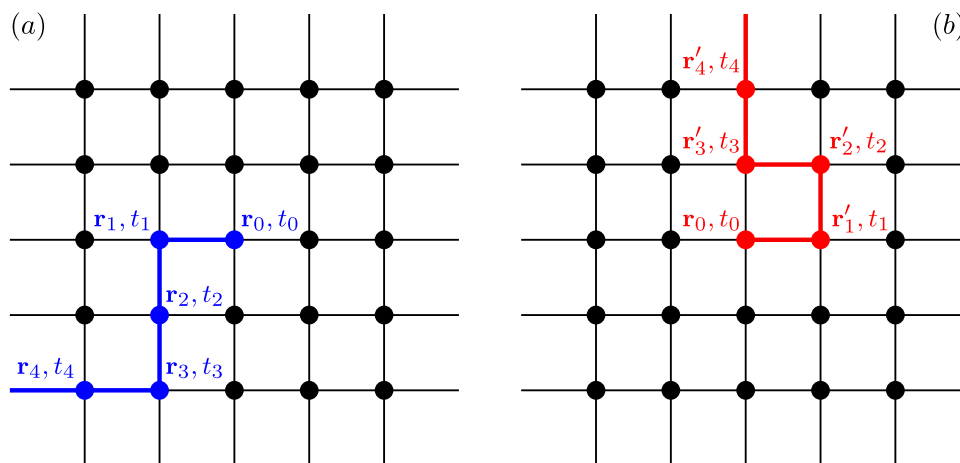
Fig. 2 Schematics of the procedure to decouple space and time. The real particle follows the blue trajectory, whereas the decoupled particle follows the red trajectory. Notice that the waiting times for both particles are the same, and they depend only on the positions of the real particle

either the temporal part or the spatial part separately or simultaneously, but leave the spatiotemporal correlations out of the picture. The reason for this is that dealing with such cross-correlations is, in general, a very complex task, even from a computational point of view.

All (semi-)analytical results usually come from applying mean-field techniques which partially or completely ignore the fine-scale structure of the system, so that some interesting features of the spatially disordered systems are not reproduced. This is the case, e.g., for the behavior of the central peak seen in the DLM [50], which is not reproduced in such pre-averaged models like the CTRW description of the DLM [50], or the minimal model of BnG [43]. It is in this regard that we seek to know to what extent the spatiotemporal correlations are responsible for the persistence of the central peak and the unusual art of convergence to a Gaussian distribution by narrowing of the central peak under rescaling $\mathbf{r} \rightarrow \mathbf{r}/\sqrt{t}$, $p \rightarrow t^{d/2}p$, instead of its lowering. To assess the effects of spatiotemporal correlations in the DLM, we remove them by randomization of step directions and see what changes by comparing the PDF in the decorrelated motion with that in the correlated one.

Let us consider a particle whose initial position is $\mathbf{r}_0$ and follow its true motion as given by a random walk scheme corresponding to the master equation (6). At that position, the particle waits for a time t_0, which is drawn from the exponential distribution $\psi(t|D_0)$ given in Eq. (11), with $D_0 = D(\mathbf{r}_0)$. Next, the particle randomly jumps to one of its neighboring lattice points, whose position is $\mathbf{r}_1$, and then waits for another time t_1, which is now drawn from the exponential distributions $\psi(t|D_1)$, with $D_1 = D(\mathbf{r}_1)$. This process of jumping and waiting is repeated until the maximal simulation time t_{max} is exceeded by the sum of waiting times. At the end, the trajectory of our particle (which we will call *real* particle to distinguish its motion from its randomized counterparts) is given by a list of positions $\{\mathbf{r}_0, \mathbf{r}_1, \mathbf{r}_2, \dots\}$, which correspond to a simple random walk, and a list $\{t_0, t_1, t_2, \dots\}$ of the correspond-

ing waiting times between subsequent jumps which are drawn from the exponential distributions $\psi(t|D_i)$ with $D_i = D(\mathbf{r}_i)$, and which are therefore dependent on the particles' positions. This dependence of the exponential distribution on the value of the local diffusion coefficient generates the spatiotemporal correlations in the DLM. The procedure to obtain the trajectories of a real particle is sketched in panel (a) of Fig. 2.

We now use the above trajectories of true motion of particles, which we refer to as "real trajectories" in what follows, to generate new trajectories in which space and time are uncorrelated. Let us start by taking the temporal part of a real trajectory, i.e., the list of waiting times $\{t_0, t_1, \dots\}$, and discard the spatial part. Then we proceed as follows: Let us consider a new particle, which we will call the *decoupled* particle, whose initial position is the same as for the real one, i.e., $\mathbf{r}_0$. The decoupled particle then waits a time equal to the first waiting time of the real particle, namely t_0, and makes a jump to one of the neighboring lattice points with position $\mathbf{r}_1'$. At this position, the decoupled particle waits a time equal to the second waiting time of the real particle, namely t_1, to make the next jump in a random direction. This process is repeated until the same number of steps as for a real particle is done, and the maximal time t_{max} is exceeded. Hence, one ends up with a trajectory for the decoupled particle consisting of a list of the positions $\{\mathbf{r}_0, \mathbf{r}_1', \mathbf{r}_2', \dots\}$ being sums of i.i.d. random steps, and *exactly the same* list of waiting times $\{t_0, t_1, \dots\}$ as for the real one, which are however decoupled from the corresponding particle's positions. This process is depicted in panel (b) of Fig. 2. The trajectories of real and decoupled particles are then used for obtaining the PDFs of displacements in a given realization of the landscape. Similar PDFs are obtained for different realizations of the diffusivity landscapes and then weighted-averaged under the equilibrium condition: the corresponding weight is proportional to the waiting time t_0 at $\mathbf{r}_0$ in the corresponding landscape.
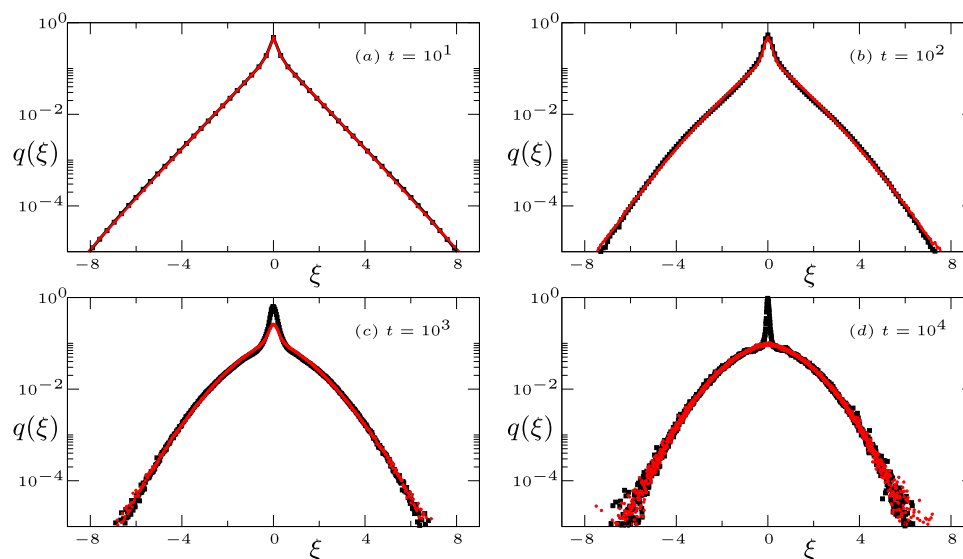
Fig. 3 A comparison of the one-dimensional cut of the PDF $q(\xi) = p(x,0)t$ of rescaled displacements $\xi = x/\sqrt{t}$ for the real particle (black) and decoupled particle (red), see text for details. Each panel represents a particular time. The flattening of the the central peak in the PDF of positions of the decoupled particle is evident at longer times

The resulting PDFs for real and decoupled particles are displayed in Fig. 3. The four panels of the plot present four different maximal times: $t_{max} = 10^1$, 10^2, 10^3, and 10^4. Each panel presents a comparison of the PDF for the real (black dots) and decoupled (red dots) particles. Each PDF is the average over 10^4 realizations of the diffusivity landscape over a lattice of 2048×2048 with $\lambda = 10$ and $D_0 = 1$. Each realization contains 10^5 particles. Plotted in Fig. 3 is a cut of PDF $p(x,y;t)$ through the origin at $y = 0$. Moreover, following [50], we plot the PDF as a function of the rescaled displacement $\xi = x/\sqrt{t}$. To keep the normalization of the PDF, it has to be rescaled as $q(\xi) = t \cdot p(\xi)$. Figure 3 shows that the decoupling of the spatial and temporal aspects of the motion changes the art of convergence to the Gaussian from the unusual one, by narrowing of the central peak, to the CLT-like convergence, by lowering and smoothening the peak.

In Refs. [48] and [50], the existence of the central peak was connected with the set of particles which started their motion in a patch with a very low local diffusivity, so that they could hardly leave the patch until very long times. The randomization results show that this is only a partial explanation, since at the beginning of its motion a decoupled particle experinces the same, very long waiting times as the real one provided it started in such a patch. The trajectory of a decoupled particle is simply a different realization of a random walk with the same starting point associated with the same list of waiting times, so that only kind of correlations which are destroyed by our procedure correspond to what happens if the particle returns to a patch with a low local diffusivity value. The real particles again experience long waiting times and therefore are sampled with a higher probability and show a tendency of accumulation in the domains with low local diffusivity

values. Such an accumulation phenomenon is clearly seen in Fig. 5 or Ref. [47]. On the other hand, decoupled particles do not show such an accumulation: new long waiting periods occur at different, random positions. Thus, it is a behaviour after an excursion that makes the peak persistent.

Figure 3, however, shows that the central peak for a decoupled motion is still present at times as long as 10^3. The reason for its existence may only be connected with correlations between waiting times along the trajectory, which are not destroyed by decoupling. Therefore, our next step will be to include the temporal correlations into a space–time decoupled CTRW model.

4 Time-correlated continuous-time random walk

Reference [50] presented a mean-field description of the DLM. This mean-field description is constructed as an *uncorrelated* CTRW model whose waiting time distribution is found by averaging the mean waiting time distribution at a site (Eq. (11)) over the distribution of the diffusion coefficients, which is given by the one-point distribution of the diffusivity landscape (Eq. (5)). This mean-field waiting time distribution is given by

$$\psi(t) = \int_0^\infty \psi(t|D)p(D)dD = \frac{5}{2}\left(\frac{3}{8}\right)^{5/2}\left(\frac{3}{8} + t\right)^{-7/2},$$
(12)

for $D_0 = 1$. The corresponding waiting time density corresponds to a Pareto type II distribution with mean waiting time $\langle t \rangle = 1/4$ and second moment $\langle t^2 \rangle = 3/8$. The fact that the initial state of the system in the DLM must be at equilibrium should also be included in its

mean-field description. This is done by taking the first waiting time to follow the PDF [59]

$$\psi_1(t) = \frac{1}{\langle t \rangle} \left[1 - \int_0^t \psi(t')dt' \right] = \frac{3}{2} \left(\frac{3}{8} \right)^{3/2} \left(\frac{3}{8} + t \right)^{-5/2},$$

(13)

which is also a Pareto type II distribution with a different exponent.

As we have shown in [50], this mean-field description, being a pre-averaged model (cf. Eq. (12)) neglecting *all* correlations, does not show any peak at the center of the distribution, except for a decaying remains of the initial condition at $\mathbf{r}(0) = 0$. The PDF of the particles' displacements in this model is shown in Fig. 5 to be compared with the results for a decoupled particle and for a CTRW model reproducing the serial correlations along the trajectory discussed below.

4.1 Correlation function of the diffusion coefficient along the trajectories

We would like to know to what extent the PDF for the decoupled particle can be replicated if temporal correlations are included. To do so, let us first determine the correlations of the diffusion coefficients along the trajectories of the random walk.

Let us start by finding an approximation for the correlation function of the diffusivity landscape $D(\mathbf{r})$ in terms of that of the correlated Gaussian field $\widehat{G}$ defined in Eq. (7). The correlation function of the diffusivity landscape is, by definition,

$$C_{DD}(\mathbf{r}) \equiv \xi(\mathbf{r}) = \frac{\langle \delta D(\mathbf{0})\delta D(\mathbf{r}) \rangle}{\sigma_D^2} = \frac{\langle D(\mathbf{0})D(\mathbf{r}) \rangle - \overline{D}^2}{\sigma_D^2},$$

(14)

with σ_D^2 the variance of the local diffusivity, and $\delta D(\mathbf{r}) = D(\mathbf{r}) - \overline{D}$. In our case, $\overline{D} = 5/3$ and $\sigma_D^2 = 10/9$, for $D_0 = 1$ in two dimensions.

Let us turn our attention to the mean $\langle D(\mathbf{0})D(\mathbf{r}) \rangle$ in the last expression of Eq. (14). Just for convenience, let us denote $D(\mathbf{0})$ and $D(\mathbf{r})$ as D_1 and D_2, respectively. By doing so, one can write

$$\langle D(\mathbf{0})D(\mathbf{r}) \rangle = \langle D_1 D_2 \rangle$$
$$= \int_0^\infty \int_0^\infty dD_1 dD_2 p(D_1, D_2; \mathbf{r}) D_1 D_2.$$

(15)

Now, we make use of the invariance of the probability measures,

$$dD_1 dD_2 p_D(D_1, D_2, \mathbf{r}) = d\widehat{G}_1 d\widehat{G}_2 p_G(\widehat{G}_1, \widehat{G}_2; \mathbf{r}),$$

with

$$p_G(\widehat{G}_1, \widehat{G}_2; \mathbf{r})$$
$$= \frac{1}{2\pi\sqrt{1 - \rho(\mathbf{r})^2}} \exp\left[-\frac{\widehat{G}_1^2 + \widehat{G}_2^2 - 2\widehat{G}_1\widehat{G}_2\rho(\mathbf{r})}{2(1 - \rho(\mathbf{r})^2)} \right]$$

being the bivariate distribution of the correlated Gaussian field used in the first stage of construction of the diffusivity landscape, with $\rho(\mathbf{r})$ being the correlation function of this field given by Eq. (7). We note that the $\mathbf{r}$-dependence in this expression is fully due to the one of the correlation function $\rho(\mathbf{r})$, and concentrate only on this ρ-dependence, introducing the function $g(\widehat{G}_1, \widehat{G}_2; \rho) = p(\widehat{G}_1, \widehat{G}_2; \mathbf{r})$. Now, we can write Eq. (15) as

$$\langle D_1 D_2 \rangle = \int_{-\infty}^\infty \int_\infty^\infty d\widehat{G}_1 d\widehat{G}_2 g(\widehat{G}_1, \widehat{G}_2; \rho) f(\widehat{G}_1) f(\widehat{G}_2),$$

(16)

with $f(\widehat{G})$ being the function that transforms the correlated Gaussian field into the diffusivity landscape, Eq. (8). Note that according to Eqs. (16) and (8), the value of the function $\langle D_1 D_2 \rangle$ is a function of ρ only, and therefore passing to the correlation function of diffusivity landscape, which differs from $\langle D(\mathbf{0})D(\mathbf{r}) \rangle$ by shift and rescaling, we see that $\xi(\mathbf{r}) = \xi[\rho(\mathbf{r})]$, and the dependence $\xi(\rho)$ is not influenced by a particular shape of the correlation function of the Gaussian landscape. Thus, the transformation from the Gaussian field to a Gamma-distributed landscape corresponds to a pointwise transformation of their correlation functions. This property will be used several times.

The integration in Eq. (16) can only be performed numerically. However, one can still find an analytical approximation to this integral. We begin by Taylor expanding the function $f(\widehat{G})$ around zero up to the fourth order:

$$f(\widehat{G}) \approx a_0 + a_1\widehat{G} + a_2\widehat{G}^2 + a_3\widehat{G}^3 + a_4\widehat{G}^4 + O(\widehat{G}^5),$$

with $a_0 = 1.4505$, $a_1 = 0.9704$, $a_2 = 0.2194$, $a_3 = 0.0130$ and $a_4 = 0.0011$ for the values of parameters used. The coefficients correspond to the numerical evaluation of the analytical expressions of the corresponding derivatives of f which is easily done with Mathematica. This last expression can now be used to compute the integral in Eq. (16) as a function of ρ, since the corresponding integral reduces to the sum of moments of a bivariate Gaussian weighted with different prefactors. Keeping contributions up to the fourth order in ρ we find

$$\langle D(\mathbf{0})D(\mathbf{r}) \rangle \approx b_0 + b_1\rho + b_2\rho^2 + b_3\rho^3 + b_4\rho^4 + O(\rho^5),$$

with $b_0 = 2.77717$, $b_1 = 1.01867$, $b_2 = 0.09043$, $b_3 = 0.00101$ and $b_4 = 0.00003$. The first coefficient (b_0) is equal to $\overline{D}^2$; therefore, it vanishes when plugging back into Eq. (14). Moreover, since the coefficients b_3 and b_4 are small compared to b_1 and b_2, they can be neglected. Under this approximation, we get $C_{DD}(\mathbf{r}) \approx \xi[\rho(\mathbf{r})]$ with the function

$$\xi(\rho) = \frac{b_1\rho + b_2\rho^2}{b_1 + b_2} = c_1\rho + c_2\rho^2, \qquad (17)$$

with $c_1 = 0.918465$ and $c_2 = 0.081535$. This simple quadratic approximation has the relative accuracy better than 0.0005 in the whole domain $0 \leq \rho \leq 1$ as compared to the result of high-precision numerical integration.

The transformation $\xi(\rho)$ is invertible, and gives therefore the possibility to construct a Gaussian field whose probability transformation would produce a Gamma-field with a desired two-point correlation function. We will use this possibility in what follows, when considering the correlated CTRW scheme in Sect. 4.2. The inverse transformation is given by the solution of the quadratic equation, giving the inverse function

$$\rho(\xi) = \sqrt{\left(\frac{c_1}{2c_2}\right)^2 + \frac{\xi}{2c_2}} - \frac{c_1}{2c_2}. \qquad (18)$$

Substituting the expression for $\rho(\mathbf{r})$, Eq. (7), into Eq. (17), we get the approximation for the correlation function of the diffusivity landscape:

$$C_{DD}(\mathbf{r}) \approx c_1 \exp\left(-\frac{\mathbf{r}^2}{2\lambda^2}\right) + c_2 \exp\left(-\frac{\mathbf{r}^2}{\lambda^2}\right). \qquad (19)$$

Now, we can use this approximation to find the correlation function of the diffusivity landscape along the trajectories, or in other words, as a function of the number of steps $C_{DD}(n)$. To do so, Eq. (19) has to be averaged using the PDF $f(\mathbf{r}|n)$ of the displacements given the number of steps n:

$$C_{DD}(n) = \int d\mathbf{r}\, C_{DD}(\mathbf{r})\, f(\mathbf{r}|n). \qquad (20)$$

Given that the spatial part of the motion is a two-dimensional simple random walk, the PDF $f(\mathbf{r}|n)$ can
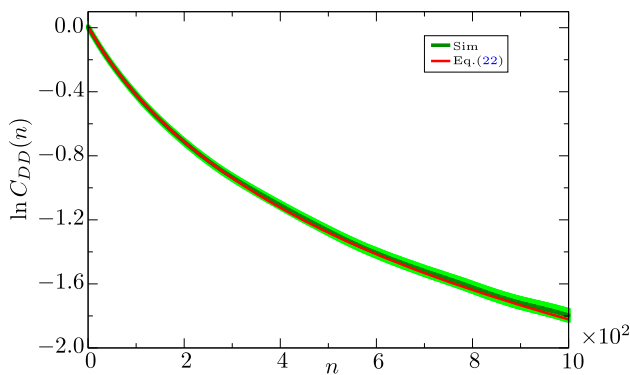
Fig. 4 Correlation function $C_{DD}(n)$ as a function of the number of steps for the two-dimensional case with $\lambda = 10$ and $D_0 = 1$. We compare the numerical results obtained in simulations of particle diffusion in the diffusivity landscapes (green line), with the approximation Eq. (22) (red line). The standard errors of the mean (SEM) are represented by the light green area. Excellent agreement is observed in the whole range of the steps' numbers

be safely approximated by a two-dimensional Gaussian distribution

$$\begin{aligned} f(\mathbf{r}|n) &= \left(\frac{d}{2\pi a^2 n}\right)^{\frac{d}{2}} \exp\left(-\frac{d\,\mathbf{r}^2}{2a^2 n}\right) \\ &= \frac{1}{2\pi\sigma^2 n} \exp\left(-\frac{\mathbf{r}^2}{2\sigma^2 n}\right), \end{aligned} \qquad (21)$$

with $d = 2$, $a = 1$ and, respectively, $\sigma^2 = 1/2$. Within this approximation, Eq. (20) takes the form

$$C_{DD}(n) \approx c_1 \left(1 + \frac{n}{2\lambda^2}\right)^{-1} + c_2 \left(1 + \frac{n}{\lambda^2}\right)^{-1}. \qquad (22)$$

Figure 4 shows a comparison between this approximate expression and the result from simulations of particle diffusion on the diffusivity landscape. Excellent agreement is observed in the whole range of steps' numbers. Note that the correlation function of diffusion coefficients is extremely long ranged.
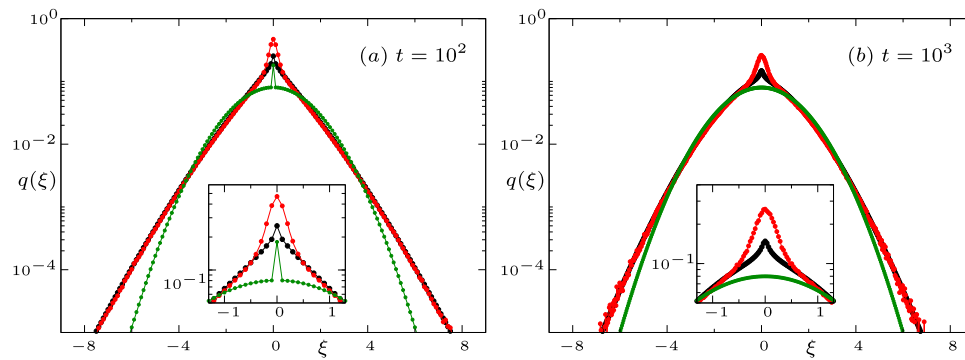
4.2 Correlated CTRW

Let us now use the correlation function of the diffusivity values along the trajectories, Eq. (22), to construct a time-correlated CTRW scheme. The process of generating correlated waiting times is similar to the one used for generating the landscape. Starting from values of $\xi(n) = C_{DD}(n)$ given by Eq. (22), we use Eq. (18) to obtain the correlation function $\rho(n)$ of a Gaussian vector, which then will be transformed to the one of diffusivity values and finally into waiting times along the trajectory.

We proceed by generating a one-dimensional uncorrelated Gaussian vector g_i by assigning to each entry of the vector a random number drawn from a Gaussian distribution with zero mean and unit variance. Then, using the Fourier filtering method [53], we generate a correlated Gaussian vector $\widehat{g}_i$ with correlation function $\rho(n)$ with $n = |i - j|$. Using the probability transformation, Eq. (8), we transform this correlated Gaussian vector into a one-dimensional array of diffusion coefficients $\mathcal{D}_i$ with the desired correlation function $C_{DD}(n) = \xi(n)$. The array of correlated diffusion coefficients $\mathcal{D}_i$ is then used to generate waiting times of our CTRW scheme by drawing random numbers t_i from an exponential waiting time distribution $\psi(t|\mathcal{D}_i) = 4\mathcal{D}_i \exp(-4\mathcal{D}_i t)$. In each realization of the process, one repeats the procedure until obtaining such a number n' of drawn elements that the sum of the first n' elements does not exceed t_{max}, but the sum of the first $n' + 1$ does. The number of elements n' is then the number of steps performed by a walker until t_{max}. The PDF of displacements for this correlated CTRW can be estimated by the average

$$p(\mathbf{r}, t_{max}) = \langle f(\mathbf{r}|n') \rangle_{n'},$$

Fig. 5 A comparison of the one-dimensional cut of the PDF $q(\xi) = p(x, 0)t$ of rescaled displacements $\xi = x/\sqrt{t}$ for the decoupled particle (red) and the correlated CTRW (black) for $t = 10^2$ and 10^3 when the differences between the behaviors are considerable. The data for the decoupled particles are the same as in Fig. 3, the result for coupled CTRW corresponds to $8 \cdot 10^6$ independent realizations, see text for details. The green dots show the results for an uncorrelated CTRW model as given by Eqs. (12) and (13)

with $f(\mathbf{r}|n)$ being the PDF of displacements for a given number of steps, Eq. (21), weighted with the waiting time of the first step.

Figure 5 shows the resulting PDF for two different times $t_{max} = 10^2$, and 10^3, one time per panel. Each panel presents a comparison between the PDF of the decoupled particle and that in the correlated CTRW. The PDFs for decoupled particles are the same as the ones in Fig. 3 for the corresponding times. For the correlated CTRW, each PDF corresponds to the average over 8×10^6 different realizations of the correlated array of diffusion coefficients $\mathcal{D}_i$, constructed with $\lambda = 10$. As one can see, both PDFs are indistinguishable in their wings, and both present a central peak which, instead of narrowing, flattens out. However, the shapes of the peaks in both cases are significantly different. We note that the uncorrelated CTRW model shows a very different behavior in the wing (its convergence to a Gaussian is much faster) and does not show any peak except for some remains of initial condition at a shorter time.

It is worth mentioning that to generate the PDFs of the correlated CTRW, we have used an extremely high number of realizations, namely 8×10^6; in our simulations, this number was subdivided into five independent runs, and the results were both considered separately and pooled for the plot in Fig. 5. The analysis of the subsets shows that the height of the peak in different sets of 1.6×10^6 realizations still fluctuates considerably, so that this height is dominated by rare events, while both in the initial model and in the decoupled variant thereof the behavior in the peak may be considered as much more typical.

Since the approximations used to construct the correlated CTRW are quite accurate and the number of realizations is high enough to guarantee sufficiently good statistics, the differences suggest that our correlated model fails to capture important details of temporal correlations. Since serial correlations along the trajectories are reproduced correctly, one can conclude that these are the higher-oder correlations that play a key

role in the development of the central peak but are of minor importance in the wings.

5 The checkerboard model

Let us now go a few steps back and consider how critical our assumption about the shape of the correlation function $\rho(\mathbf{r})$, Eq. (7), is, i.e., what happens if this function is chosen differently. To do so, we consider a DLM with a checkerboard-like diffusivity landscape. On a lattice, a checkerboard-like diffusivity landscape consists of an array of $N \times N$ squares containing $2\zeta \times 2\zeta$ lattice points. A constant diffusion coefficient $D^{(i)}$ is assigned to each square. These diffusion coefficients are drawn from the distribution given by Eq. (5), the condi-
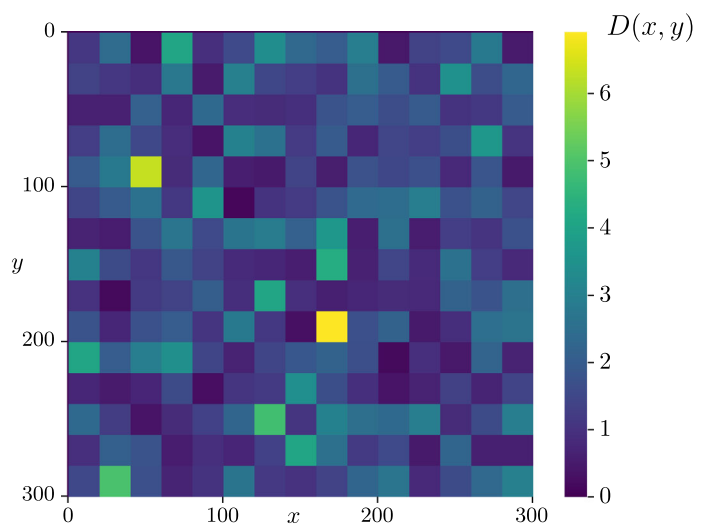
Fig. 6 A two-dimensional realization of the diffusivity landscape $D(\mathbf{r})$ for the checkerboard model. It corresponds to a 300×300 lattice, where each cell has a size of 2ζ with $\zeta = 10$, and sampled diffusion coefficient is $D_0 = 1$
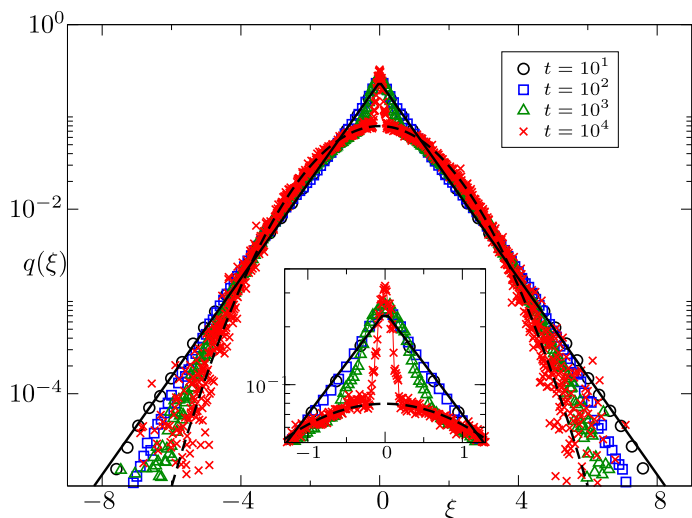
Fig. 7 A one-dimensional cut of the PDF $q(\xi) = p(x,0)t$ of rescaled displacements $\xi = x/\sqrt{t}$ for the diffusion of particles in the checkerboard model. The straight line corresponds to the Laplace distribution, whereas the dotted line corresponds to the Gaussian distribution. The inset shows a close-up of the central part of the distribution exposing the peak

tion needed for the diffusion to be BnG. This choice of diffusivity landscape strongly changes the shape of the correlation function. Moreover, the changes in diffusion coefficients on the borders of the squares are now discontinuous, while the previous diffusivity landscape was assumed to model a smooth situation. In this model, ζ defines the correlation length of the landscape; to compare to the results of the above DLM, we set $\zeta = \lambda$. Figure 6 shows one realization of the checkerboard-like diffusivity landscape on a lattice of 300×300 with $\zeta = 10$ and $D_0 = 1$.

As in the case of the DLM, we perform random walk simulations of particles diffusing on an ensemble of checkerboard-like landscapes, from which the PDF of displacements can then be constructed. Figure 7 shows the time evolution of the PDF averaged over 2×10^4 different realizations of the landscape, each one using 10^4 particles. The landscape was constructed with $N = 109$ and $\zeta = 10$, i.e., we consider a lattice of size 2180×2180. One can see that the central peak is preserved. Moreover, the transition to the Gaussian limits follows the same type of convergence by its narrowing. This suggests that the form of the correlation function of the diffusivity landscape does not change the overall behavior. A closer look, though, reveals the presence of some discontinuities near the center of the distribution, which are expected from the fact that the diffusivity landscape itself is discontinuous.

6 Conclusions

In this work, we study the diffusivity landscape model (DLM) characterized by a diffusion coefficient slowly varying in space. Under specific conditions, this model leads to a Brownian, yet non-Gaussian diffusion, that is, the MSD is linear in time, but the shape of the PDF changes from a Laplace distribution at short times to a Gaussian distribution at long ones. The art of convergence to the Gaussian is quite a peculiar one, since the PDF at all times displays a central peak that does not decay with time, but narrows under rescaling. We show that the persistence of the peak is due to strong spatiotemporal correlations introduced by correlations of local diffusion coefficients in space. Destroying the spatiotemporal correlations on the level of single trajectories (by considering a different relaization of steps' directions while keeping the same list of waiting times as for the real motion) lets the peak to lower and to disappear at longer times. This kind of behavior is qualitatively reproduced by a correlated CTRW model with serial correlations of waiting times along the trajectory mimicking the ones observed in simulations. The model, however, fails to quantitatively reproduce the PDF for the decoupled case, showing a considerably lower peak. We attribute this fact to an important role of higher-order correlations which are not reproduced by the model. By considering a different variant of correlated disorder (the checkerboard model), we moreover show that the existence of the peak is insensitive to the exact shape of the correlation function of local diffusivities, and its shape is hardly sensitive to it.

Author contributions

All authors contributed equally to the paper.

Data availability statement This manuscript has no associated data or the data will not be deposited. [Authors' comment: This is a theoretical study with no experimental data. All numerical data generated during this study are available on reasonable request.].

Declarations

Conflict of interest The authors have no conflicts to disclose.

References

1. R. Brown, XXVII. A brief account of microscopical observations made in the months of June, July and August 1827, on the particles contained in the pollen of plants; and on the general existence of active molecules in organic and inorganic bodies. The Philosophical Magazine **4**(21), 161–173 (1828) https://doi.org/10.1080/14786442808674769

2. A. Einstein, Über die von der molekularkinetischen Theorie der Wärme geforderte Bewegung von in ruhenden Flüssigkeiten suspendierten Teilchen. Ann. Phys. **322**(8), 549–560 (1905). https://doi.org/10.1002/andp.19053220806

3. R. Maiocchi, The case of Brownian motion. Br. J. Hist. Sci. **23**(3), 257–283 (1990)

4. V. Balakrishnan, *Elements of Nonequilibrium Statistical Mechanics* (Springer, Cham, 2020)

5. J.B. Perrin, *Atoms* (Constable, London, 1916)

6. M. Smoluchowski, Zur kinetischen Theorie der Brownschen Molekularbewegung und der Suspensionen. Ann. Phys. **326**(14), 756–780 (1906). https://doi.org/10.1002/andp.19063261405

7. M.V. Smoluchowski, Über Brownsche Molekularbewegung unter Einwirkung äußerer Kräfte und deren zusammenhang mit der verallgemeinerten Diffusionsgleichung. Ann. Phys. **353**(24), 1103–1112 (1916). https://doi.org/10.1002/andp.19163532408

8. P. Langevin, Sur la théorie du mouvement Brownien. C. R. Acad. Sci. (Paris) **146**, 530–533 (1908)

9. R. Metzler, J. Klafter, The random walk's guide to anomalous diffusion: a fractional dynamics approach. Phys. Rep. **339**(1), 1–77 (2000). https://doi.org/10.1016/S0370-1573(00)00070-3

10. I.M. Sokolov, Models of anomalous diffusion in crowded environments. Soft Matter **8**, 9043–9052 (2012). https://doi.org/10.1039/C2SM25701G

11. F. Höfling, T. Franosch, Anomalous transport in the crowded world of biological cells. Rep. Prog. Phys. **76**(4), 046602 (2013). https://doi.org/10.1088/0034-4885/76/4/046602

12. D. Krapf, Chapter five - mechanisms underlying anomalous diffusion in the plasma membrane. In: Kenworthy, A.K. (ed.) Lipid Domains. Current Topics in Membranes, vol. 75, pp. 167–207. Academic Press, New York (2015). https://doi.org/10.1016/bs.ctm.2015.03.002 . https://www.sciencedirect.com/science/article/pii/S1063582315000034

13. F.A. Oliveira, R.M.S. Ferreira, L.C. Lapas, M.H. Vainstein, Anomalous diffusion: A basic mechanism for the evolution of inhomogeneous systems. Frontiers in Physics **7** (2019) https://doi.org/10.3389/fphy.2019.00018

14. W. Wang, R. Metzler, A.G. Cherstvy, Anomalous diffusion, aging, and nonergodicity of scaled Brownian motion with fractional Gaussian noise: overview of related experimental observations and models. Phys. Chem. Chem. Phys. **24**, 18482–18504 (2022). https://doi.org/10.1039/D2CP01741E

15. P. Massignan, C. Manzo, J.A. Torreno-Pina, M.F. García-Parajo, M. Lewenstein, G.J. Lapeyre, Nonergodic subdiffusion from brownian motion in an inhomogeneous medium. Phys. Rev. Lett. **112**, 150603 (2014). https://doi.org/10.1103/PhysRevLett.112.150603

16. I. Goychuk, V.O. Kharchenko, R. Metzler, Persistent sinai-type diffusion in gaussian random potentials with decaying spatial correlations. Phys. Rev. E **96**, 052134 (2017). https://doi.org/10.1103/PhysRevE.96.052134

17. I. Goychuk, Viscoelastic subdiffusion in a random gaussian environment. Phys. Chem. Chem. Phys. **20**, 24140–24155 (2018). https://doi.org/10.1039/C8CP05238G

18. I. Goychuk, T. Pöschel, Finite-range viscoelastic subdiffusion in disordered systems with inclusion of inertial effects. New J. Phys. **22**(11), 113018 (2020). https://doi.org/10.1088/1367-2630/abc603

19. B. Wang, S.M. Anthony, S.C. Bae, S. Granick, Anomalous yet Brownian. Proc. Natl. Acad. Sci. **106**(36), 15160–15164 (2009). https://doi.org/10.1073/pnas.0903554106

20. K.C. Leptos, J.S. Guasto, J.P. Gollub, A.I. Pesci, R.E. Goldstein, Dynamics of enhanced tracer diffusion in suspensions of swimming eukaryotic microorganisms. Phys. Rev. Lett. **103**, 198103 (2009). https://doi.org/10.1103/PhysRevLett.103.198103

21. H. Kurtuldu, J.S. Guasto, K.A. Johnson, J.P. Gollub, Enhancement of biomixing by swimming algal cells in two-dimensional films. Proc. Natl. Acad. Sci. **108**(26), 10391–10395 (2011). https://doi.org/10.1073/pnas.1107046108

22. B. Wang, J. Kuo, S.C. Bae, S. Granick, When Brownian diffusion is not Gaussian. Nat. Mater. **11**(6), 481–485 (2012). https://doi.org/10.1038/nmat3308

23. M.J. Skaug, J. Mabry, D.K. Schwartz, Intermittent molecular hopping at the solid-liquid interface. Phys. Rev. Lett. **110**, 256101 (2013). https://doi.org/10.1103/PhysRevLett.110.256101

24. C. Yu, J. Guan, K. Chen, S.C. Bae, S. Granick, Single-molecule observation of long jumps in polymer adsorption. ACS Nano **7**(11), 9735–9742 (2013). https://doi.org/10.1021/nn4049039

25. K. He, F. Babaye Khorasani, S.T. Retterer, D.K. Thomas, J.C. Conrad, R. Krishnamoorti, Diffusive dynamics of nanoparticles in arrays of nanoposts. ACS Nano **7**(6), 5122–5130 (2013). https://doi.org/10.1021/nn4007303

26. J. Guan, B. Wang, S. Granick, Even hard-sphere colloidal suspensions display Fickian yet non-Gaussian diffusion. ACS Nano **8**(4), 3331–3336 (2014). https://doi.org/10.1021/nn405476t

27. A.L. Thorneywork, D.G.A.L. Aarts, J. Horbach, R.P.A. Dullens, On the Gaussian approximation in colloidal hard sphere fluids. Soft Matter **12**, 4129–4134 (2016). https://doi.org/10.1039/C5SM03049H

28. W. He, H. Song, Y. Su, L. Geng, B.J. Ackerson, H.B. Peng, P. Tong, Dynamic heterogeneity and non-Gaussian statistics for acetylcholine receptors on live cell

membrane. Nat. Commun. **7**(1), 11701 (2016). https://doi.org/10.1038/ncomms11701

29. S. Acharya, U.K. Nandi, S. Maitra Bhattacharyya, Fickian yet non-Gaussian behaviour: A dominant role of the intermittent dynamics. The Journal of Chemical Physics **146**(13) (2017) https://doi.org/10.1063/1.4979338 . 134504

30. C.E. Wagner, B.S. Turner, M. Rubinstein, G.H. McKinley, K. Ribbeck, A rheological study of the association and dynamics of MUC5AC gels. Biomacromol **18**(11), 3654–3664 (2017). https://doi.org/10.1021/acs.biomac.7b00809

31. I. Chakraborty, G. Rahamim, R. Avinery, Y. Roichman, R. Beck, Nanoparticle mobility over a surface as a probe for weak transient disordered peptide-peptide interactions. Nano Lett. **19**(9), 6524–6534 (2019). https://doi.org/10.1021/acs.nanolett.9b02764

32. T. Kwon, O.-S. Kwon, H.-J. Cha, B.J. Sung, Stochastic and heterogeneous cancer cell migration: Experiment and theory. Sci. Rep. **9**(1), 16297 (2019). https://doi.org/10.1038/s41598-019-52480-3

33. I. Chakraborty, Y. Roichman, Disorder-induced Fickian, yet non-Gaussian diffusion in heterogeneous media. Phys. Rev. Research **2**, 022020 (2020). https://doi.org/10.1103/PhysRevResearch.2.022020

34. R. Pastore, A. Ciarlo, G. Pesce, F. Greco, A. Sasso, Rapid Fickian yet non-Gaussian diffusion after subdiffusion. Phys. Rev. Lett. **126**, 158003 (2021). https://doi.org/10.1103/PhysRevLett.126.158003

35. R. Pastore, A. Ciarlo, G. Pesce, A. Sasso, F. Greco, A model-system of Fickian yet non-Gaussian diffusion: light patterns in place of complex matter. Soft Matter **18**, 351–364 (2022). https://doi.org/10.1039/D1SM01133B

36. M. Hidalgo-Soria, E. Barkai, Hitchhiker model for laplace diffusion processes. Phys. Rev. E **102**, 012109 (2020). https://doi.org/10.1103/PhysRevE.102.012109

37. M. Hidalgo-Soria, E. Barkai, S. Burov, Cusp of non-gaussian density of particles for a diffusing diffusivity model. Entropy **23**(2) (2021) https://doi.org/10.3390/e23020231

38. E. Barkai, S. Burov, Packets of diffusing particles exhibit universal exponential tails. Phys. Rev. Lett. **124**, 060603 (2020). https://doi.org/10.1103/PhysRevLett.124.060603

39. W. Wang, E. Barkai, S. Burov, Large deviations for continuous time random walks. Entropy **22**(6) (2020) https://doi.org/10.3390/e22060697

40. A. Pacheco-Pozo, I.M. Sokolov, Large deviations in continuous-time random walks. Phys. Rev. E **103**, 042116 (2021). https://doi.org/10.1103/PhysRevE.103.042116

41. M.V. Chubynsky, G.W. Slater, Diffusing diffusivity: A model for anomalous, yet Brownian, diffusion. Phys. Rev. Lett. **113**, 098302 (2014). https://doi.org/10.1103/PhysRevLett.113.098302

42. R. Jain, K.L. Sebastian, Diffusion in a crowded, rearranging environment. J. Phys. Chem. B **120**(16), 3988–3992 (2016). https://doi.org/10.1021/acs.jpcb.6b01527

43. A.V. Chechkin, F. Seno, R. Metzler, I.M. Sokolov, Brownian yet non-Gaussian diffusion: From superstatistics to subordination of diffusing diffusivities. Phys. Rev. X

7, 021002 (2017). https://doi.org/10.1103/PhysRevX.7.021002

44. Y. Lanoiselée, D.S. Grebenkov, A model of non-Gaussian diffusion in heterogeneous media. J. Phys. A: Math. Theor. **51**(14), 145602 (2018). https://doi.org/10.1088/1751-8121/aab15f

45. J. Slezak, R. Metzler, M. Magdziarz, Superstatistical generalised langevin equation: non-Gaussian viscoelastic anomalous diffusion. New J. Phys. **20**(2), 023026 (2018). https://doi.org/10.1088/1367-2630/aaa3d4

46. W. Wang, F. Seno, I.M. Sokolov, A.V. Chechkin, R. Metzler, Unexpected crossovers in correlated random-diffusivity processes. New J. Phys. **22**(8), 083041 (2020). https://doi.org/10.1088/1367-2630/aba390

47. E.B. Postnikov, A. Chechkin, I.M. Sokolov, Brownian yet non-Gaussian diffusion in heterogeneous media: from superstatistics to homogenization. New J. Phys. **22**(6), 063046 (2020). https://doi.org/10.1088/1367-2630/ab90da

48. L. Luo, M. Yi, Non-Gaussian diffusion in static disordered media. Phys. Rev. E **97**, 042122 (2018). https://doi.org/10.1103/PhysRevE.97.042122

49. L. Luo, M. Yi, Quenched trap model on the extreme landscape: The rise of subdiffusion and non-gaussian diffusion. Phys. Rev. E **100**, 042136 (2019). https://doi.org/10.1103/PhysRevE.100.042136

50. A. Pacheco-Pozo, I.M. Sokolov, Convergence to a Gaussian by narrowing of central peak in Brownian yet non-Gaussian diffusion in disordered environments. Phys. Rev. Lett. **127**, 120601 (2021). https://doi.org/10.1103/PhysRevLett.127.120601

51. T.A. Pirey, L.F. Cugliandolo, V. Lecomte, F. Wijland, Path integrals and stochastic calculus. Advances in Physics , 1–85 (2023). https://doi.org/10.1080/00018732.2023.2199229

52. I.M. Sokolov, Ito, stratonovich, hänggi and all the rest: The thermodynamics of interpretation. Chemical Physics **375**(2), 359–363 (2010) https://doi.org/10.1016/j.chemphys.2010.07.024 . Stochastic processes in Physics and Chemistry (in honor of Peter Hänggi)

53. R. Toral, P. Colet, *Stochastic Numerical Methods: An Introduction for Students and Scientists* (Wiley-VCH, Weinheim, 2014)

54. J.W. Haus, K.W. Kehr, Diffusion in regular and disordered lattices. Phys. Rep. **150**(5), 263–406 (1987). https://doi.org/10.1016/0370-1573(87)90005-6

55. J.-P. Bouchaud, A. Georges, Anomalous diffusion in disordered media: Statistical mechanisms, models and physical applications. Phys. Rep. **195**(4), 127–293 (1990). https://doi.org/10.1016/0370-1573(90)90099-N

56. A.V. Chechkin, M. Hofmann, I.M. Sokolov, Continuous-time random walk with correlated waiting times. Phys. Rev. E **80**, 031112 (2009). https://doi.org/10.1103/PhysRevE.80.031112

57. V. Tejedor, R. Metzler, Anomalous diffusion in correlated continuous time random walks. J. Phys. A: Math. Theor. **43**(8), 082002 (2010). https://doi.org/10.1088/1751-8113/43/8/082002

58. J.H.P. Schulz, A.V. Chechkin, R. Metzler, Correlated continuous time random walks: combining scale-invariance with long-range memory for spatial and temporal dynamics. J. Phys. A: Math. Theor. **46**(47),

475001 (2013). https://doi.org/10.1088/1751-8113/46/47/475001

59. J. Klafter, I.M. Sokolov, First Steps in Random Walks: From Tools to Applications. Oxford University Press, Oxford (2011). https://books.google.de/books?id=y4BNxvImzTkC